Chinese Chemical Letters 31 (2020) 1243–1247

Contents lists available at ScienceDirect

Chinese Chemical Letters

journal homepage: www.elsevier.com/locate/cclet

Communication

Design a thieno[3,2-*b*]thiophene bridged nonfullerene acceptor to increase open-circuit voltage, short-circuit current-density and fill factor *via* the ternary strategy

Xiaofang Li[a,b,1], Kun Li[b,c,1], Dan Su[a,b], Fugang Shen[a,b,*], Shuying Huo[a,*], Hongbing Fu[c], Chuanlang Zhan[a,b,*]

[a] College of Chemistry and Environmental Science, Hebei University, Baoding 071002, China
[b] CAS key Laboratory of Photochemistry, Institute of Chemistry, Chinese Academy of Sciences, Beijing 100190, China
[c] Department of Chemistry, Capital Normal University, Beijing 100048, China

ARTICLE INFO

Article history:
Received 5 September 2019
Received in revised form 15 October 2019
Accepted 24 October 2019
Available online 30 October 2019

Keywords:
Fullerene-free
Polymer solar cell
Small molecule acceptor
Ternary solar cell
Organic photovoltaic

ABSTRACT

In this study, we report a new small molecule acceptor (named TT-4F) which uses 3,6-dimethoxylthieno [3,2-*b*]thiophene (TT) as the π-bridge. Addition of 0.05 weight ratio amount of TT-4F into the host binary blend of PTB7-Th:IEICO-4F, resulting in a ternary blend in a weight ratio of 1:1:0.05, enables increased open-circuit voltage (V_{oc}), short-circuit current-density (J_{sc}), and fill-factor (FF) at the same time. Finally, 12.1% efficiency is obtained. Compared to the 3-(2-ethylhexyloxylthiophene) bridge on IEICO-4F, the additional methoxyl group on the TT-6 position is involved in the lowest unoccupied molecular orbital (LUMO) and the larger π-system on TT increases the electron-donating nature, both of which help to raise the LUMO level, one reason of the increased V_{oc}. Upon addition of 0.05 TT-4F, the hole mobility is increased, the monomolecular recombination is reduced, and the charge dissociation and collection is enhanced. All of these contribute to the increased J_{sc} and FF.

Fullerene-free polymer solar cell (PSC) uses nonfullerene small molecule as the electron acceptor material and polymer as the electron donor material. As potential stocks for clean renewable energy in the future, PSCs have been widely recognized by the academic community because PSC has the advantages of low-cost, semi-transparency, mechanical-flexibility and large-area production. In the past several decades, various types of organic solar cells have emerged in an endless stream, and have achieved gratifying results. More than 15% of power conversion efficiencies (PCEs) have been recently reported due to the emergence of new non-fullerene materials [1–6], such as the fused-benzothiadiazole based acceptor, named Y6 (2,2′-((2*Z*,2′*Z*)-(12,13-bis(2-ethylhexyl)-3,9-diundecyl-12,13-dihydro-[1,2,5]thiadiazolo[3,4-*e*]thieno [2,"3″:4′,5′]thieno[2′,3′:4,5]pyrrolo[3,2-*g*]thieno[2′,3′:4,5]thieno [3,2-*b*]indole-2,10-diyl)bis(methanylylidene))-bis(5,6-difluoro-3-oxo-2,3-dihydro-1*H*-indene-2,1-diylidene)dimalononitrile) [7].

However, due to the inherent drawbacks of organic photovoltaic materials, such as narrow absorption, low charge mobilities, and strong recombination, ternary approach has been received increasing attention [8–15]. Along with the fast advances on the nonfullerene small-molecule acceptors and the fullerene-free PSCs, people began to turn their attention to the ternary blended material systems that contain a polymer donor and two non-fullerene acceptors. In this ternary blended system, the second acceptor (the guest) has to comply with the aggregation of the host acceptor so as to maintain the film-morphology of the host binary blend [16]. Normally, an acceptor having a narrower bandgap than the host was selected as the acceptor guest to cover a wider wavelength range of the near infrared solar emission spectrum, by which an increased short-circuit current-density (J_{sc}) can be obtained [17–27]. However, the lowest unoccupied molecular orbital (LUMO) energy level of the acceptor guest has to be reduced to achieve the reduced optical bandgap. The lower-lying LUMO level inevitably reduces the open-circuit voltage (V_{oc}) [28–30], which can result in reduced efficiency in most cases. To overcome the issue of the reduced V_{oc} value, another strategy with the use of a higher-LUMO-level acceptor guest (than the host) to obtain an increased V_{oc} value has been proposed by us recently [31]. Due to the improvement of the film-morphology, increased J_{sc} and

* Corresponding authors at: College of Chemistry and Environmental Science, Hebei University, Baoding 071002, China.
E-mail addresses: shenfg@hbu.edu.cn (F. Shen), shuyinghuo@hbu.edu.cn (S. Huo), clzhan@iccas.ac.cn (C. Zhan).
[1] These two authors contributed equally to this work.

https://doi.org/10.1016/j.cclet.2019.10.029

fill-factor (FF) can be simultaneously achieved in some of the cases reported recently [4,16,31–35]. Nevertheless, the cases showing the features of the "V_{oc}-increased" approach are yet much less than the cases having characteristics of the "J_{sc}-increased" strategy.

In this study, we design and synthesized a new nonfullerene small molecule acceptor, named TT-4F (Fig. 1a), as the acceptor guest of the known binary host of PTB7-Th:IEICO-4F [36] (Fig. 1a). The resulted ternary system shows the simultaneous increase in V_{oc}, J_{sc} and FF. To raise the energy levels of the highest occupied molecular orbital (HOMO) and LUMO, we replaced the thiophene on IEICO-4F with the larger π-system, thieno[3,2-*b*]thiophene (TT), and functionalized the TT-3,6 positions with two methoxyl groups. With these modifications, the Frontier molecular orbitals energy levels of TT-4F meet the requirements as the acceptor guest: the LUMO level of TT-4F is higher than the LUMO of IEICO-4F and its HOMO positions between the HOMOs of PTB7-Th and IEICO-4F. The tests on the solar cells indicate that TT-4F can be used as the third component of PTB7-Th:IEICO-4F to fabricate the ternary blended solar cell. The addition of 0.05 wt ratio amount of TT-4F, resulting in a weight ratio of 1:1:0.05, supplies the optimal device with V_{oc} = 0.709 V, J_{sc} = 25.05 mA/cm^2, FF = 68.08%, and PCE = 12.12% in comparison to the PCE of 11.46% of the host binary device.

Fig. 1b shows the optimized conformations and the LUMO and HOMO distributions of TT-4F and IEICO-4F calculated using the density functional theory (DFT). The backbones of both acceptor molecules are coplanar. The dihedral angle (Table S1 in Supporting information) between the IDT core and the bridge is 3.6° and 7.73° for TT-4F and IEICO-4F, respectively. The dihedral angle between the bridge and end IC-2 F is 5.25° and 0.47° for TT-4 F and IEICO-4F, respectively. Compared to IEICO-4F, the involvement of the TT in the HOMO and LUMO expands the electron delocalization of the π-electrons, helping to raise the HOMO and LUMO levels. For TT-

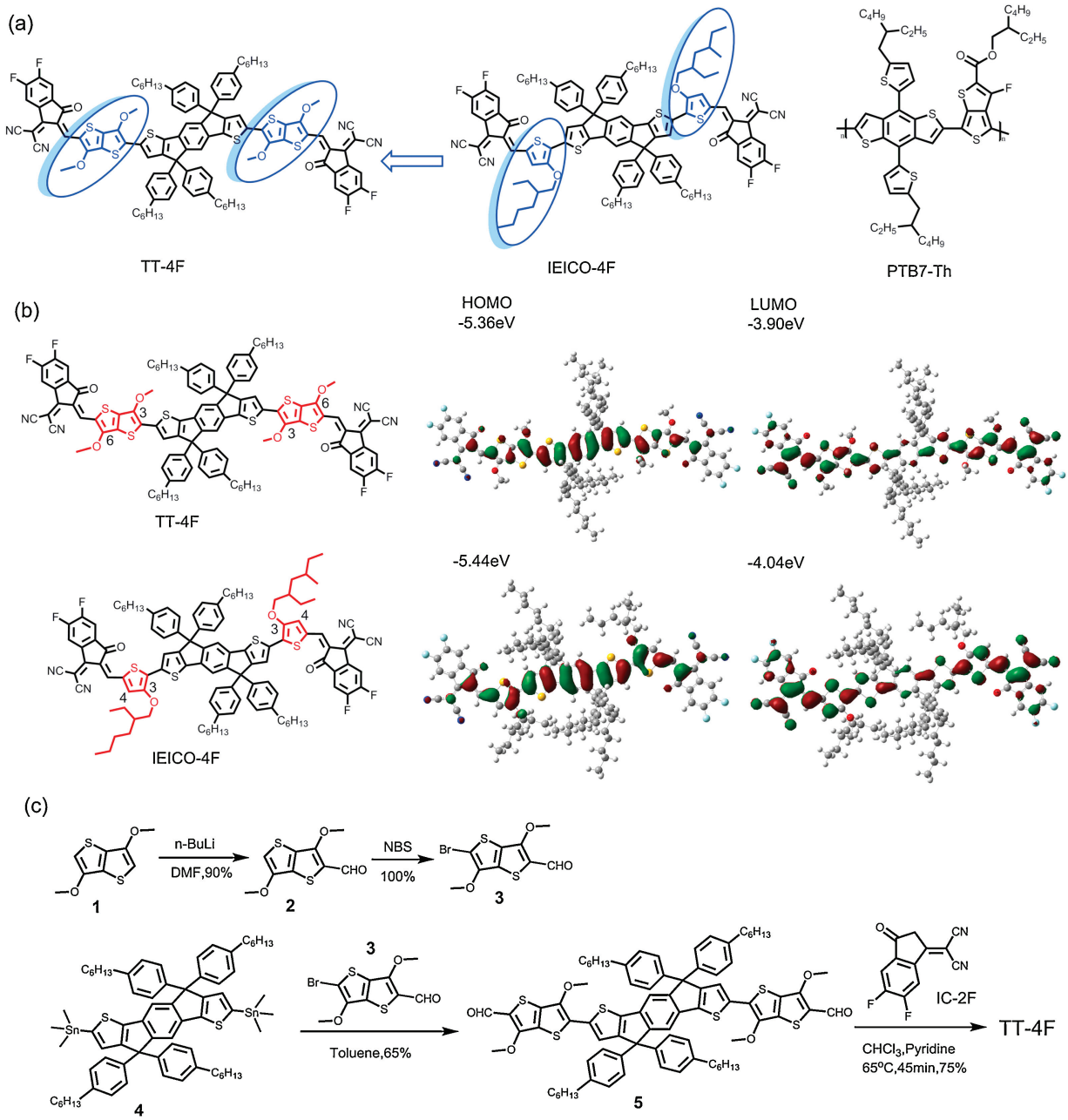

Fig. 1. (a) Chemical structures of PTB7-Th, IEICO-4F and TT-4F. (b) The optimized conformations and the distributions of the HOMO and LUMO of TT-4F and IEICO-4F. (c) Synthetic routes to TT-4F.

4F, the 6-methoxyl is included in the LUMO, which is again benefited for the raising of the LUMO level. However, the 6-methoxyl is a node of the HOMO of TT-4F, contributing less to the acceptor HOMO. In contrast, the 3-methoxyl is involved in the acceptor HOMO, while is a node of the LUMO, and hence, contributes to the acceptor HOMO, while not to the LUMO. For the acceptor that has a higher LUMO level, the upshifting of the HOMO is important because it helps to reduce the bandgap.

The synthetic route of TT-4F is shown in Fig. 1c. We first introduced an aldehyde group on 3,6-dimethoxythieno[3,2-*b*]-thiophene that was then brominated to yield compound **3**. Compound **3** was then coupled with 4,4,9,9-tetrakis(4-hexylphenyl)-4,9-dihydro-sindaceno[1,2-b:5,6-*b*′]dithiophene-2,7-diyl) bis(trimethylstannane) by following the Still coupling reaction to give compound **5**. Finally, the terminal group IC-2F was connected, and the target molecule TT-4F was obtained. As shown in the Fig. S1 (Supporting information), the decomposition temperature (5% weight loss) was about 371 °C. This good thermal property is sufficient to make organic solar cells.

The UV–vis absorption spectrum of the TT-4F solution is given in Fig. S2 (Supporting information) and the spectra of the neat films of the donor and acceptor materials are shown in Fig. 2a. In the solution, the absorption peak appears at 737 nm and the maximum molar extinction coefficient (ε_{max}) is 1.86×10^{-5} L mol^{-1} cm^{-1} (Table S2 in Supporting information). In thin film, the absorption peak is seen at 792 nm and the maximum absorptivity is 3.15×10^{5} cm^{-1}. The absorption onset of the neat film is located at 900 nm, corresponding to an optical bandgap (E_g^{opt}) of 1.38 eV.

The cyclic voltammetry (CV) was used to measure the energy levels of the donor and the acceptors (Fig. S3 in Supporting information). Fig. 2b shows the energy level diagram of the donor and the acceptors. The LUMO levels of PBT7-Th, TT-4F, and IEICO-4F are -3.64 eV, -3.90 eV and -4.04 eV, respectively. The HOMO levels are -5.24 eV, -5.36 eV, -5.44 eV, respectively. First, the LUMO energy level of TT-4F is higher than the LUMO of IEICO-4F by 0.14 eV, while lower than the LUMO of PTB7-Th by 0.26 eV. Second, the HOMO level of TT-4F is higher than the HOMO of IEICO-4F by 0.08 eV and lower than the HOMO of PTB7-Th by 0.04 eV, meaning that TT-4F can be used as the acceptor guest of the PTB7-Th:IEICO-4F to fabricate the ternary solar cell.

All solar cells were prepared using the conventional structure ITO/PEDOT:PSS/active layer/PDINO/Al. Here, PDINO is amino *N*-oxide perylene diimide. Since the solubility of TT-4F in chlorobenzene is poor, the binary solar cell with PTB7-Th:TT-4F as the active layer cannot be fabricated. Interestingly, when a small amount of TT-4F (0.05 and 0.1) was blended with PTB7-Th:IEICO-4F (1:1), the ternary solar cell worked. The optimizations using 1-cholonaphthanlene (CN) are shown in Table S3 (Supporting information). The current density–voltage (*J*–*V*) characteristic curves are shown in Fig. 2c and the corresponding device parameters are summarized in Table 1. The ternary device based on PTB7-Th : TT-4F : IEICO-4F showed a PCE of 12.12%, a V_{oc} of 0.709 V, a J_{sc} of 25.05 mA/cm^2 and an FF of 68.08%. In comparison to the PTB7-Th:IEICO-4F based binary device, a higher V_{oc}, a larger J_{sc}, and a higher FF are simultaneously obtained with the use of 0.05 weight ratio amount of TT-4F as the acceptor guest, which suggests that TT-4F be a good regulator of electric property and film-morphology of the PTB7-Th:IEICO-4F binary blend. The external quantum efficiency (EQE) spectra of the optimized binary and ternary devices are shown in Fig. 2d. Both the EQE spectra cover the wavelength range of 300–1000 nm. The J_{sc} integrated from the EQE spectrum of the ternary device is 24.09 mA/cm^2, which is well consistent with the J_{sc} value obtained from the *J*-*V* curve (error <5%).

Table 1
Photovoltaic data of the binary and ternary solar cells. All data were obtained under illumination of AM 1.5 G (100 mW/cm^2) light source.

PBT7-Th:IEICO-4F:TT-4F	J_{sc} (mA/cm^2)	V_{oc} (V)	FF (%)	PCE (%)
1:1:0	24.50	0.703	66.88	11.46
1:1:0.05	25.05	0.709	68.08	12.12
1:1:0.1	23.00	0.702	64.55	10.46

To see the effects of the addition of 0.05 wt ratio amount of TT-4F on the charge mobilities, we measured the electron (μ_e) and hole (μ_h) mobilities with the space charge limited current (SCLC) method [37–41]. The device structure for measuring the electron mobility is ITO/titanium(diisopropanol)bis(2,4-pentanedione) (TIPD)/active layer/PDINO/Al, and for measuring the hole mobility, the device structure is ITO/PEDOT:PSS/active layer/Au. The dark *J*–*V* data are given in Fig. 3a. For the host binary blend, $\mu_e = 1.40 \times 10^{-3}$ cm^2 V^{-1} s^{-1} and $\mu_h = 1.25 \times 10^{-3}$ cm^2 V^{-1} s^{-1}. For the ternary blend, $\mu_e = 1.69 \times 10^{-3}$ cm^2 V^{-1} s^{-1} and $\mu_h = 1.53 \times 10^{-3}$ cm^2 V^{-1} s^{-1}. It can be clearly seen that the μ_h is increased with the addition of 0.05 TT-4F as the acceptor guest, which accounts for the increased J_{sc}.

We again studied the recombination mechanisms by measuring the light intensity (P_{light}) dependent *J*–*V* characteristics. The

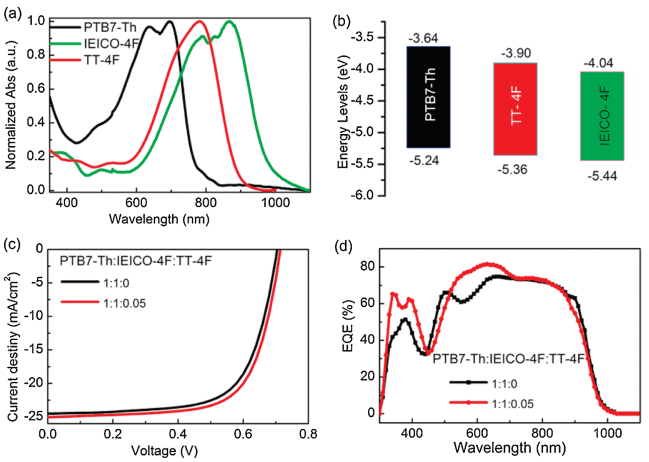

Fig. 2. Absorption spectra (a) and energy level diagram (b) of neat films of the polymer and nonfullerene acceptors. The energy levels were measured using thin film deposited on the work electrode surface under the same conditions. The *J*–*V* curves (c) and EQE spectra (d) of the optimized binary and ternary solar cells.

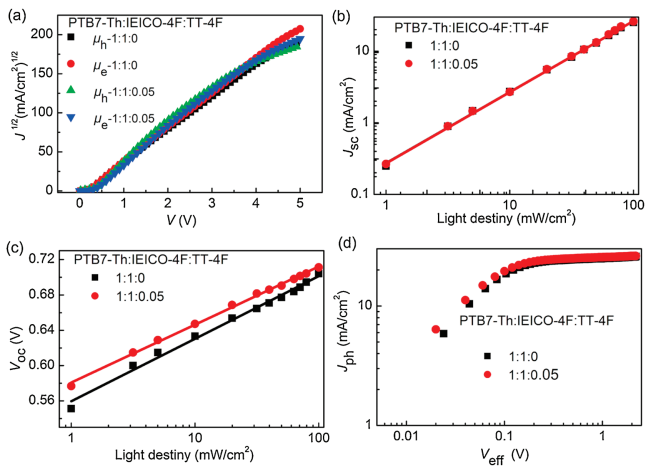

Fig. 3. Dark *J*–*V* curves for calculations of hole and electron mobilities (a). Plots of V_{oc} (b) and J_{sc} (c) *versus* incident light intensity and J_{ph} *vs.* V_{eff} characteristics (d) of the optimal binary and ternary devices.

recombination mechanisms can be reflected by plotting the J_{sc} and V_{oc} as a function of P_{light} according to the Eqs.: $\log J_{sc} \propto \alpha \log P_{light}$ and $V_{oc} \propto (nKT/q)\ln P_{light}$, where k, T, and q are the Boltzmann constant, temperature in Kelvin, and the elementary charge, respectively. For both the binary and ternary devices, the fitting α value is close to 1 (Fig. 3b), which indicates that the bimolecular recombination can be negligible [42–46]. The fitting n value (Fig. 3c) is 1.18 kT/q and 1.10 kT/q for the binary and ternary device, respectively. The smaller n value in the ternary device than the host binary solar cell indicates that weak monomolecular recombination is involved, which accounts for the increased FF in comparison to the host binary device.

We also measured the photocurrent density (J_{ph}) as a function of effective voltage (V_{eff}) to gain an understanding of exciton dissociation and charge extraction. Fig. 3d shows the plots of J_{ph} *versus* V_{eff} of the binary and ternary devices. Here, J_{ph} is the difference between the dark current-density and illuminated current-density measured from the same one solar cell device, respectively, and V_{eff} is the difference of build-in potential and the applied voltage with the build-in potential obtained when $J_{ph} = 0$. We can see that at the high applied voltage ($V_{eff} > 2.2$ V), J_{ph} is approaching to saturation, indicating that almost all photo-generated excitons are dissociated and free charge carriers are efficiently collected by the electrodes [47–50]. With the use of 0.05 wt ratio amount of TT-4F, the charge dissociation and collection becomes more efficient. The charge collection efficiency at short-circuit is 96.7% and 94.9% estimated from the ternary and binary devices, respectively. The ternary device shows higher charge collection efficiency.

Taken together, the studies demonstrate that with the use of TT-4F as the acceptor guest, the hole mobility is increased, the monomolecular at open-circuit is reduced, the charge dissociation and collection efficiency can be enhanced. All of these reflect that the TT-4F is a good regulator of the electric property of the host binary blend.

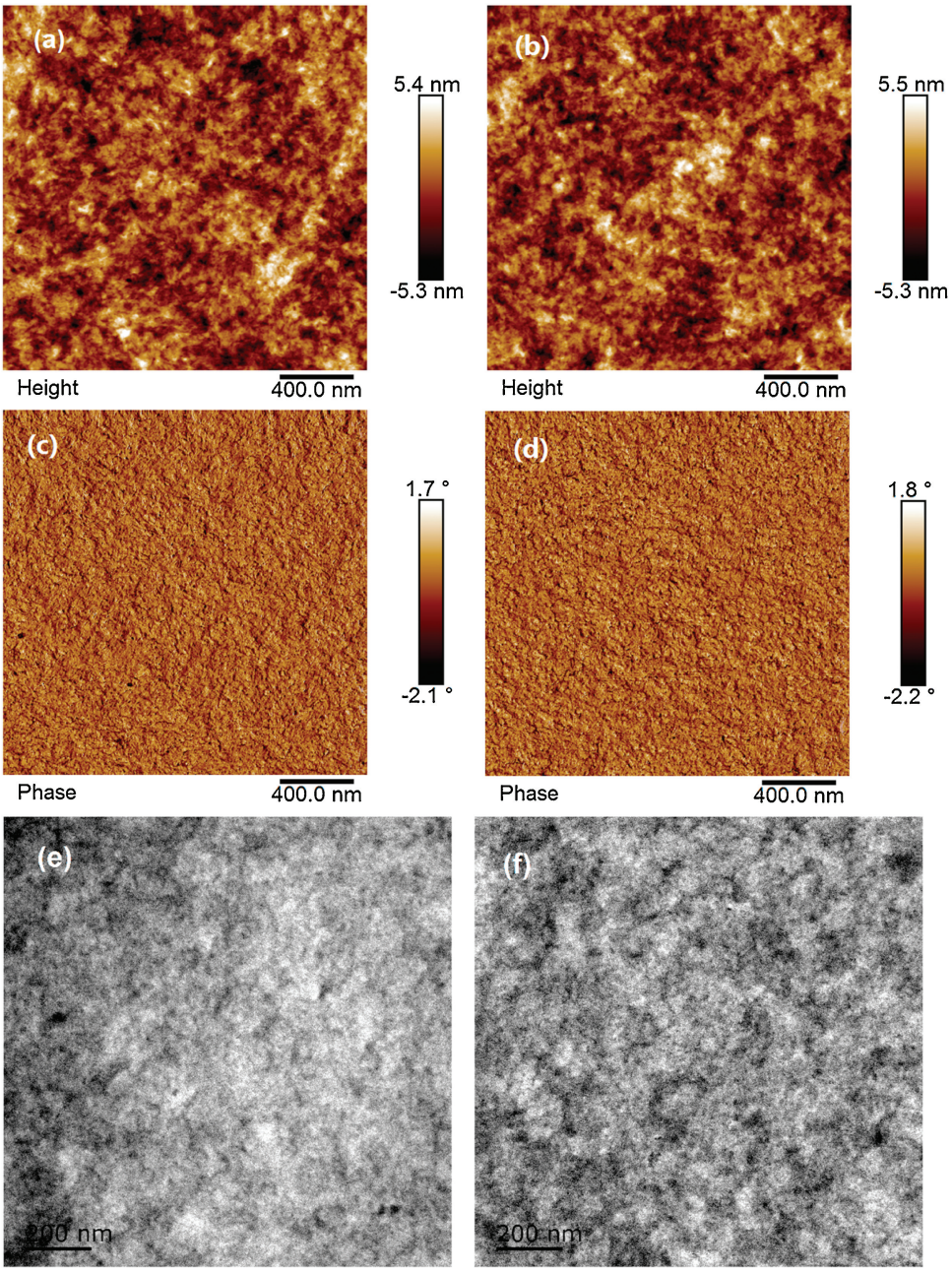

Fig. 4. AFM height (a,b) and phase (c,d) and TEM (e,f) images of the binary (a,c,e) and ternary (b,d,f) blended solar cell films.

Now we go to see the change of film-morphology after addition of TT-4F. The atomic force microscopy (AFM) and transmission electron microscopy (TEM) are given in Fig. 4. The AFM images indicate that the nanoscaled interpenetrating film-morphology and fine phase-separation of the host binary blend are well maintained after the addition of 0.05 weight amount of TT-4F. The well maintenance of the morphology can be explained by the structural similarity of the TT-4F with the host IEICO-4F. In the AFM images, the fibril dark domains (acceptor-rich phases) in the height image are corresponding to the fibril phase domains painted in a deeper brown colour. We can see that longer fibril dark domains are more frequently seen in the ternary blend. The root mean square (RMS) roughness values are 1.51 nm and 1.79 nm for the binary and ternary blends, respectively. Nanoscaled phase-separated fine film-morphology is also characterized in TEM. Compared to the TEM image of the host binary, first, the morphology is well kept. Second, larger and longer dark phases (acceptor-rich phases) are more frequently seen in the ternary blend.

In summary, we have synthesized a new small-molecule acceptor, named TT-4F, with 3,6-dimethoxylthieno[3,2-*b*]thiophene as the bridge. The use of TT-4F as the acceptor guest of PTB7-Th:IEICO-4F achieves an increased V_{oc}, J_{sc}, and FF at the same time. Finally, 12.1% efficiency is obtained from the ternary solar cell. The increase of V_{oc} is due to the higher-lying LUMO level as a result of the incorporation of the larger π-system bridge on TT-4F than IEICO-4F and the substitution of methoxyl group on the TT-6 position that is involved in the LUMO of TT-4F. The increase in J_{sc} and FF can be due to the increased hole mobility, reduced monomolecular recombination, and enhanced charge dissociation and collection.

Declaration of competing interest

The authors declare that they have no known competing financial interests or personal relationships that could have appeared to influence the work reported in this paper.

Acknowledgments

The authors gratefully acknowledge the financial support from the National Natural Science Foundation of China (NSFC, Nos. 91433202, 21773262 and 21327805), Natural Science Foundation of Hebei Province (No. B2016201014).

References

[1] B. Fan, D. Zhang, M. Li, et al., Sci. China Chem. 62 (2019) 746–752.
[2] X. Xu, K. Feng, Z. Bi, et al., Adv. Mater. 9 (2019) e1901872.
[3] Y. Cui, H. Yao, J. Zhang, et al., Nat. Commun. 10 (2019) 2515.
[4] M.A. Pan, T.K. Lau, Y. Tang, et al., J. Mater. Chem. A 7 (2019) 20713–20722.
[5] Y. Ma, X. Zhou, D. Cai, et al., Mater. Horizon. 7 (2020) 117–124.
[6] D. Su, M.A. Pan, Z. Liu, et al., Chem. Mater. 31 (2019) 8908–8917.
[7] J. Yuan, Y. Zhang, L. Zhou, et al., Joule 3 (2019) 1–12.
[8] Q. An, J. Zhang, W. Gao, et al., Small 14 (2018) e1802983.
[9] P. Cheng, R. Wang, J. Zhu, et al., Adv. Mater. 30 (2018) 1705243.
[10] J. Gao, R. Ming, Q. An, et al., Nano Energy 63 (2019) 103888.
[11] L. Nian, Y. Kan, H. Wang, et al., Energy Environ. Sci. 11 (2018) 3392–3399.
[12] L. Zhong, H. Bin, Y. Li, et al., J. Mater. Chem. A 6 (2018) 24814–24822.
[13] Z. Li, D. Tang, Z. Ji, et al., J. Mater. Chem. C 6 (2018) 9119–9129.
[14] X. Xu, Z. Bi, W. Ma, et al., J. Mater. Chem. A 7 (2019) 14199–14208.
[15] W. Liu, J. Yao, C. Zhan, Chin. Chem. Lett. 28 (2017) 875–880.
[16] Y. Chang, T.K. Lau, M.A. Pan, et al., Mater. Horizon. 6 (2019) 2094–2102.
[17] W. Wu, G. Zhang, X. Xu, et al., Adv. Funct. Mater. 28 (2018) 1707493.
[18] R. Yu, S. Zhang, H. Yao, et al., Adv. Mater. 29 (2017) 1700437.
[19] M. Xiao, K. Zhang, S. Dong, et al., ACS Appl. Mater. Interfaces 10 (2018) 25594–25603.
[20] L. Zhan, S. Li, H. Zhang, et al., Adv. Sci. 5 (2018) 1800755.
[21] J. Lee, S.J. Ko, M. Seifrid, et al., Adv. Energy Mater. 8 (2018) 1801209.
[22] P. Xue, Y. Xiao, T. Li, et al., J. Mater. Chem. A 6 (2018) 24210–24215.
[23] S. Dai, Y. Xiao, P. Xue, et al., Chem. Mater. 30 (2018) 5390–5396.
[24] L. Yang, W. Gu, L. Hong, et al., ACS Appl. Mater. Interfaces 9 (2017) 26928–26936.
[25] X. Xu, Z. Bi, W. Ma, et al., Adv Mater. 29 (2017) 1704271.
[26] Y. Chang, X. Zhang, Y. Tang, et al., Nano Energy 64 (2019) 103934.
[27] X. Ma, W. Gao, J. Yu, et al., Energy Environ. Sci. 11 (2018) 2134–2141.
[28] M. Zhang, W. Gao, F. Zhang, et al., Energy Environ. Sci. 11 (2018) 841–849.
[29] P. Cheng, J. Wang, Q. Zhang, et al., Adv. Mater. 30 (2018) 1801501.
[30] B. Kan, Y.Q.Q. Yi, X. Wan, et al., Adv. Energy Mater. 8 (2018) 1800424.
[31] K. Li, Y. Wu, Y. Tang, et al., Adv. Energy Mater. 9 (2019) 1901728.
[32] W. Su, Q. Fan, X. Guo, et al., Nano Energy 38 (2017) 510–517.
[33] Z. Hu, F. Zhang, Q. An, et al., ACS Energy Lett. 3 (2018) 555–561.
[34] W. Jiang, R. Yu, Z. Liu, et al., Adv. Mater. 30 (2018) 1703005.
[35] T. Liu, Z. Luo, Q. Fan, et al., Energy Environ. Sci. 11 (2018) 3275–3282.
[36] H. Yao, Y. Cui, R. Yu, et al., Angew. Chem. In. Ed. 56 (2017) 3045–3049.
[37] W. Huang, S.Y. Chang, P. Cheng, et al., Nano Lett. 18 (2018) 7977–7984.
[38] T. Liu, Y. Guo, Y. Yi, et al., Adv. Mater. 28 (2016) 10008–10015.
[39] J. Lee, S.J. Ko, M. Seifrid, et al., Adv. Energy Mater. 8 (2018) 1801212.
[40] M. Zhang, W. Gao, F. Zhang, et al., Energy Environ. Sci. 11 (2018) 841–849.
[41] M. Zhang, Z. Xiao, W. Gao, et al., Adv. Energy Mater. 8 (2018) 1801968.
[42] X. Ma, W. Gao, J. Yu, et al., Energy Environ. Sci. 11 (2018) 2134–2141.
[43] J. Zhang, G. Xu, F. Tao, et al., Adv. Mater. (2019) e1807159.
[44] Y. Li, J.D. Lin, X. Che, et al., J. Am. Chem. Soc. 139 (2017) 17114–17119.
[45] L. Yang, W. Gu, L. Hong, et al., ACS Appl. Mater. Interfaces 9 (2017) 26928–26936.
[46] Y. Liu, S. Wang, Y. Tao, et al., Chin. Chem. Lett. 27 (2016) 1250–1258.
[47] P. Ye, Y. Chen, J. Wu, et al., J. Mater. Chem. C 5 (2017) 12591–12596.
[48] F. Ullah, H. Chen, Ch. Li, Chin. Chem. Lett. 28 (2017) 503–511.
[49] P. He, X. Qiao, Q. Qian, et al., Chin. Chem. Lett. 27 (2016) 1277–1282.
[50] X. Shen, G. Han, Y. Yi, Chin. Chem. Lett. 27 (2016) 1453–1463.